The effect of quantum confinement and discrete dopants in nanoscale 50 nm n-MOSFETs: a three-dimensional simulation

Gianluca Fiori
Dipartimento di Ingegneria dell'Informazione: Elettronica, Informatica, Telecomunicazioni, Università di Pisa
Giuseppe Iannaccone
Dipartimento di Ingegneria dell'Informazione: Elettronica, Informatica, Telecomunicazioni, Università di Pisa

G. Fiori, G. Iannaccone, "*The effect of quantum confinement and discrete dopants in nanoscale 50 nm n-MOSFETs: a three-dimensional simulation*", Nanotechnology, **13** , 3, pp.294-298 (2002).

INSTITUTE OF PHYSICS PUBLISHING NANOTECHNOLOGY
Nanotechnology **13** (2002) 294–298 PII: S0957-4484(02)31502-2

The effect of quantum confinement and discrete dopants in nanoscale 50 nm n-MOSFETs: a three-dimensional simulation

G Fiori and G Iannaccone

Dipartimento di Ingegneria dell'Informazione, Università degli studi di Pisa, Via Diotisalvi 2, I-56122, Pisa, Italy

E-mail: g.fiori@iet.unipi.it and g.iannaccone@iet.unipi.it

Received 4 December 2001, in final form 27 February 2002
Published 23 May 2002
Online at stacks.iop.org/Nano/13/294

Abstract
In this paper, we investigate the effects of quantum confinement at the $Si–SiO_2$ interface on the properties of MOSFETs with a channel length of 50 nm. To this end, we have developed a three-dimensional Poisson–Schrödinger solver, based on an approximation which allows us to decouple the Schrödinger equation into an equation in the direction perpendicular to the channel and an equation in the plane of the channel. This code is able to provide the MOSFET transport properties for very small drain-to-source voltage. We have also evaluated the effects of the discrete distribution of dopants on the dispersion of threshold voltage, by simulating a large number of devices with uniform nominal doping profile but with different actual 'atomistic' distributions of impurities.

1. Introduction

The so-called 'well-tempered' MOSFETs, proposed by Antoniadis[1], are benchmark device structures useful for investigating effects typical of nanoscale dimensions on the properties of future generations of MOSFETs, and for comparing predictions and capabilities of specific codes for technological computer-aided design (TCAD).

The reduced gate oxide thickness and the increased bulk doping, required to control short-channel effects, cause a high electric field in the direction perpendicular to the Si/SiO_2 interface, strongly confining charge carriers in the channel and splitting the density of states in the channel into well-separated two-dimensional subbands [1, 2]. Therefore, semiclassical models are no longer suitable for describing sub-0.1 μm MOSFETs. The effect of quantum confinement on MOSFET threshold voltage has been investigated by Fiegna and Abramo [3] for a one-dimensional MOS structure. In [4] a two-dimensional self-consistent model has been used to simulate n-MOS transistors, while in [5] the charge distribution in ultrasmall MOSFETs has been computed by solving the two-dimensional Schrödinger equation. However, to also include the effect of the discrete distribution of impurities, a three-dimensional simulation must be performed.

We have developed a code for the simulation in three dimensions of MOSFETs with ultrashort channels, taking into account quantum confinement in the channel and depletion of the polysilicon gate. The Poisson–Schrödinger equation has been discretized on a rectangular grid with the box-integration method and solved using the Newton–Raphson algorithm. While meshless methods with arbitrary point placement might be advantageous for the simulation of the effects due to random impurities [6], a rectangular grid allows us to solve the Schrödinger equation in a convenient way.

We present results for the so-called 'well-tempered' bulk Si n-MOSFETs with channel length and width of 50 nm. As we shall show, quantum confinement increases the threshold voltage by up to 140 mV.

We have also considered the effects of the random distribution of dopants on the threshold voltage. Indeed, as the scaling down of device geometries reaches deep-submicrometre dimensions, the number of doping atoms in the depletion region is of the order of hundreds.

[1] http://www-mtl.mit.edu/Well

Consequently, intrinsic fluctuations of the number and of the position of the atoms strongly influence the value of the threshold voltage, as pointed out in several papers [7–10]. Here, we will take into account both the effect of random dopants, by performing a three-dimensional simulation, and the effect of quantum confinement on threshold voltage.

2. Model

The potential profile in the three-dimensional simulation domain shown in figure 2 (later) obeys the Poisson equation

$$\vec{\nabla}\cdot[\epsilon(\vec{r})\,\vec{\nabla}\phi(\vec{r})] = -q[p(\vec{r}) - n(\vec{r}) + N_D^+(\vec{r}) - N_A^-(\vec{r})], \quad (1)$$

where ϕ is the electrostatic potential, ϵ is the dielectric constant, p and n are the hole and electron densities, respectively, N_D^+ is the concentration of ionized donors and N_A^- is the concentration of ionized acceptors. While hole, acceptor and donor densities are computed in the whole domain with the semiclassical approximation, the electron concentration, in regions where confinement is strong, needs to be computed by solving the Schrödinger equation with the density functional theory. The observation that quantum confinement is strong only along the direction perpendicular to the Si/SiO_2 interface has led us to decouple the Schrödinger equation into a one-dimensional equation in the vertical (x) direction and a two-dimensional equation in the y–z plane: the density of states in the horizontal plane is well approximated by the semiclassical expression, since there is no in-plane confinement, while discretized states appear in the vertical direction.

The expression for the single-particle Schrödinger equation is three dimensional, with the anisotropic effective mass

$$-\frac{\hbar^2}{2}\frac{\partial}{\partial x}\frac{1}{m_x}\frac{\partial}{\partial x}\Psi - \frac{\hbar^2}{2}\frac{\partial}{\partial y}\frac{1}{m_y}\frac{\partial}{\partial y}\Psi - \frac{\hbar^2}{2}\frac{\partial}{\partial z}\frac{1}{m_z}\frac{\partial}{\partial z}\Psi + V\Psi = E\Psi. \quad (2)$$

We can arbitrarily write the wavefunction $\Psi(x, y, z)$ as

$$\Psi(x, y, z) = \psi(x, y, z)\chi(y, z). \quad (3)$$

Substituting (3) in (2), we obtain the following expression:

$$-\frac{\hbar^2}{2}\chi\frac{\partial}{\partial x}\frac{1}{m_x}\frac{\partial}{\partial x}\psi - \left[\frac{\hbar^2}{2}\frac{\partial}{\partial y}\frac{1}{m_y}\frac{\partial}{\partial y} + \frac{\hbar^2}{2}\frac{\partial}{\partial z}\frac{1}{m_z}\frac{\partial}{\partial z}\right]\psi\chi + V\psi\chi = E\psi\chi, \quad (4)$$

where the dependence on x, y and z is implicit. We assume that $\psi(x, y, z)$ is weakly dependent on y and z (we will discuss this point in the following section) and take ψ as the solution of the Schrödinger equation along the x-direction:

$$-\frac{\hbar^2}{2}\frac{\partial}{\partial x}\frac{1}{m_x}\frac{\partial}{\partial x}\psi + V\psi = E_1(y, z)\psi. \quad (5)$$

Equation (4) can be written as

$$-\left[\frac{\hbar^2}{2}\frac{\partial}{\partial y}\frac{1}{m_y}\frac{\partial}{\partial y} + \frac{\hbar^2}{2}\frac{\partial}{\partial z}\frac{1}{m_z}\frac{\partial}{\partial z}\right]\psi\chi + \left[-\frac{\hbar^2}{2}\frac{\partial}{\partial x}\frac{1}{m_x}\frac{\partial}{\partial x}\psi + V\psi\right]\chi = E\psi\chi; \quad (6)$$

by substituting (5) in (6) we obtain

$$-\left[\frac{\hbar^2}{2}\frac{\partial}{\partial y}\frac{1}{m_y}\frac{\partial}{\partial y} + \frac{\hbar^2}{2}\frac{\partial}{\partial z}\frac{1}{m_z}\frac{\partial}{\partial z}\right]\psi\chi + E_1(y, z)\psi\chi = E\psi\chi. \quad (7)$$

Finally, the weak dependence of $\psi(x, y, z)$ on y and z reduces equation (7) to

$$-\left[\frac{\hbar^2}{2}\frac{\partial}{\partial y}\frac{1}{m_y}\frac{\partial}{\partial y} + \frac{\hbar^2}{2}\frac{\partial}{\partial z}\frac{1}{m_z}\frac{\partial}{\partial z}\right]\chi + E_1(y, z)\chi = E\chi. \quad (8)$$

Since $E_1(y, z)$ in the cases considered is rather smooth in the y–z plane, we will assume that the eigenvalues of equation (8) essentially obey the two-dimensional semiclassical density-of-states equation.

The confining potential V can be written as $V = E_C + V_{exc}$, where E_C is the conduction band and V_{exc} is the exchange–correlation potential within the local density approximation [11]:

$$V_{exc} = -\frac{q^2}{4\pi^2\varepsilon_0\varepsilon_r}[3\pi^3 n(\vec{r})]^{1/3}. \quad (9)$$

Anisotropy of the electron effective mass in silicon must be taken into account: the Schrödinger equation is solved considering the effective masses along the three directions in k-space. The electron density in confined regions therefore becomes

$$n(x) = \frac{2k_BTm_t}{\pi\hbar^2}\sum_i |\psi_{li}|^2 \ln\left[1 + \exp\left(\frac{E_F - E_{li}}{k_BT}\right)\right] + \frac{4k_BT\sqrt{m_lm_t}}{\pi\hbar^2}\sum_i |\psi_{ti}|^2 \ln\left[1 + \exp\left(\frac{E_F - E_{ti}}{k_BT}\right)\right], \quad (10)$$

where ψ_{li}, E_{li}, ψ_{ti} and E_{ti} are the eigenfunctions and eigenvalues obtained from the one-dimensional Schrödinger equation using the longitudinal effective mass m_l and the transverse effective mass m_t, respectively.

To solve the Poisson–Schrödinger equation self-consistently, we have used the Newton–Raphson method with a predictor/corrector algorithm similar to that proposed in [12]. In particular, the Schrödinger equation is not solved at each Newton–Raphson iteration step. Indeed, if we consider the eigenfunctions constant within a loop and the eigenvalues varied by a quantity of about $q(\phi - \tilde{\phi})$, where $\tilde{\phi}$ is the potential used to solve the Schrödinger equation and ϕ is the potential at the current iteration, then the electron density becomes

$$n(x) = \frac{2k_BTm_t}{\pi\hbar^2} \times \sum_i |\psi_{li}|^2 \ln\left[1 + \exp\left(\frac{E_F - E_{li} + q(\tilde{\phi} - \phi)}{k_BT}\right)\right] + \frac{4k_BT\sqrt{m_lm_t}}{\pi\hbar^2} \times \sum_i |\psi_{ti}|^2 \ln\left[1 + \exp\left(\frac{E_F - E_{ti} + q(\tilde{\phi} - \phi)}{k_BT}\right)\right]. \quad (11)$$

The algorithm is then repeated cyclically until the norm of $\phi - \tilde{\phi}$ is smaller than a predetermined value. In the worst case, convergence is achieved in <15 iterations of the Newton–Raphson method in the inner cycle and five solutions of the Schrödinger equation.

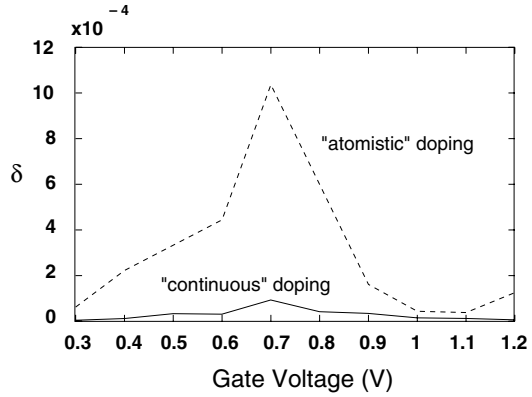

Figure 1. A plot of δ defined as in equation (14) as a function of V_{GS} for a 'continuous' doping profile and for an 'atomistic' doping profile.

3. Validation of the approximate solution of the Schrödinger equation

The aim of the present section is to demonstrate that by decoupling the three-dimensional Schrödinger equation we introduce only a negligible error. Let us define the operator

$$\hat{T}_{yz} \equiv -\frac{\hbar^2}{2}\frac{\partial}{\partial y}\frac{1}{m_y}\frac{\partial}{\partial y} - \frac{\hbar^2}{2}\frac{\partial}{\partial z}\frac{1}{m_z}\frac{\partial}{\partial z}, \tag{12}$$

and let us call the term that we have neglected in passing from (7) to (8) $a(x, y, z)$:

$$a(x, y, z) \equiv \hat{T}_{yz}\psi\chi - \psi\hat{T}_{yz}\chi; \tag{13}$$

if the approximation is valid, $a(x, y, z)$ must be much smaller than $E - E_{1i}(y, z)$ at any point of the domain, which means that the parameter δ, which we define as

$$\delta \equiv \max_{x,y,z}\left|\frac{a(x, y, z)}{[E - E_{1i}(y, z)]\psi(x, y, z)\chi(y, z)}\right| \tag{14}$$

must be much smaller than 1.

Since χ obeys the two-dimensional density-of-states equation, it can be written as $\chi = Ae^{j(k_y y + k_z z)}$, where

$$\frac{\hbar^2 k_y^2}{2m_y} + \frac{\hbar^2 k_z^2}{2m_z} = E - E_{1i}. \tag{15}$$

In order to consider the worst case, we consider the low-lying subband, where $m_y = m_z = m_t$, where m_t is the effective transverse mass, and $k_y = 0$ and $k_z = \sqrt{2m_t(E - E_{1i})}/\hbar$, because the potential is more rapidly varying in the z-direction than in the y-direction.

In figure 1 we plot delta as a function of the gate voltage for a 'continuous' doping profile (solid curve) and for an 'atomistic' doping profile (dashed curve): in both cases δ is smaller than 10^{-3}.

4. Results and discussion

As anticipated in the introduction, the device considered is a so-called 'well-tempered' MOSFET with channel length of 50 nm. The simulation domain is illustrated in figure 2 and the doping profile is shown in figure 3. Source and drain doping profiles are Gaussian, while the superhalo doping is implanted in the channel in order to reduce charge-sharing effects that become important in short-channel geometries.

The increase of the threshold voltage V_T due to quantum confinement has been evaluated quantitatively for the MOSFET structure considered.

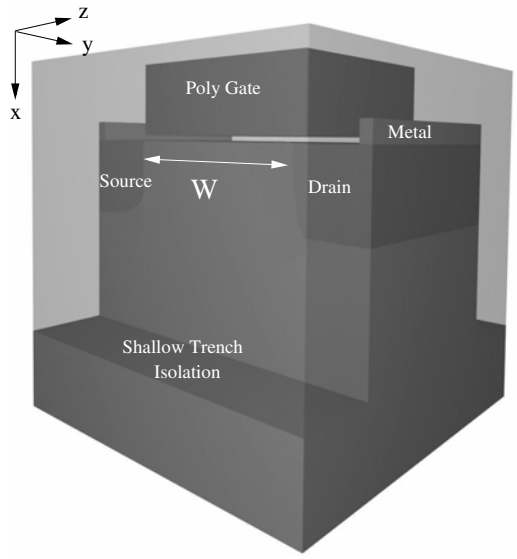

Figure 2. The three-dimensional structure of the simulated MOSFETs.

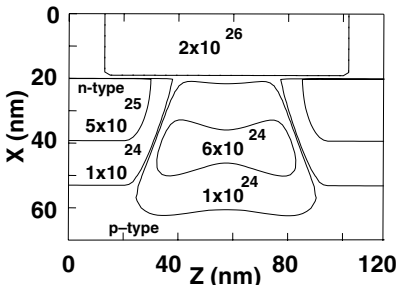

Figure 3. The difference between the donor and acceptor concentrations for the 50 nm MOSFET considered.

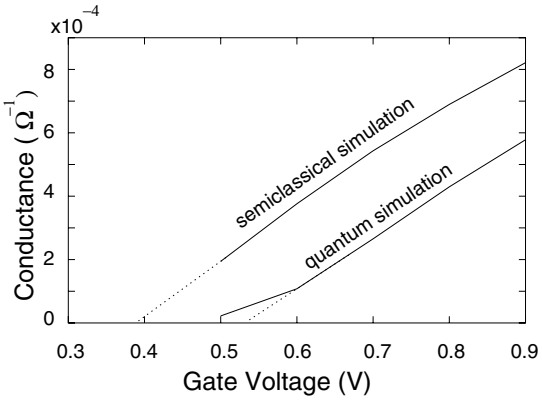

Figure 4. Conductance as a function of V_{GS} computed with semiclassical and quantum models.

For small drain-to-source voltage V_{DS} and gate voltage $V_{GS} > V_T$, the channel conductance g_0 has the following approximate expression:

$$g_0 \equiv \left.\frac{\partial I_D}{\partial V_{DS}}\right|_{V_{DS}=0} \approx \mu_n \frac{W}{L} C_{ox}(V_{GS} - V_T) \qquad (16)$$

where μ_n is the electron mobility in the channel and C_{ox} is the oxide capacitance per unit area. For this reason, V_T can be obtained as the intercept of the g_0–V_{GS} curve in the strong-inversion region with the V_{GS}-axis.

The assumption of zero V_{DS} is a limitation of our approach and does not allow us to take into account drain-induced barrier lowering. In addition, the definition of V_T that we use can give a different value compared to other commonly used definitions [1]. However, we believe that our evaluation of the V_T-shift due to quantum confinement is quantitatively accurate.

In figure 4 the g_0–V_{GS} curves computed with quantum and semiclassical simulations are depicted. As can be seen, the difference between the V_T computed with semiclassical and quantum models is very significant and close to 140 mV. Indeed, as the quantum confinement becomes relevant, discrete energy levels higher than the bottom of the conduction band appear: a large gate voltage is therefore required to induce channel inversion.

The conductance is computed as follows. In the drift-diffusion model the current density can be written as

$$\vec{J}_n = -qn\mu_n \vec{\nabla}\phi + q D_n \vec{\nabla} n \qquad (17)$$

where D_n is the electron diffusion coefficient.

If ϕ_0 is the potential profile computed with $V_{DS} = 0$, equation (17) becomes

$$0 = -qn_0\mu_n \vec{\nabla}\phi_0 + q D_n \vec{\nabla} n_0, \qquad (18)$$

where n_0 is the electron density at equilibrium.

For a very small perturbation from the equilibrium, we can write $\phi = \phi' + \phi_0$ and $n = n' + n_0$, and expand the difference between equations (17) and (18) to first order in ϕ'. For weak to strong inversion, the main term is

$$\vec{J}_n = -qn_0\mu_n \vec{\nabla}\phi'. \qquad (19)$$

The continuity equation $\vec{\nabla} \cdot \vec{J}_n = 0$ gives us

$$\vec{\nabla} \cdot (n_0 \vec{\nabla}\phi') = 0. \qquad (20)$$

We solve the above equation in a region of the MOSFET containing the channel, as shown in figure 5. If we apply a small voltage $\Delta\phi$ between the surfaces in the source and drain regions, and zero current density through the lateral faces of the region, we have the boundary conditions illustrated in figure 5. For simplicity we assume constant mobility $\mu_n = 700\ \mathrm{cm^2\ V^{-1}\ s^{-1}}$.

4.1. Threshold voltage dispersion

As MOSFET scaling approaches the sub-100 nm regime, the number of impurity atoms is of the order of hundreds in the channel depletion region. Intrinsic dopant fluctuations determine a significant dispersion of the threshold voltage.

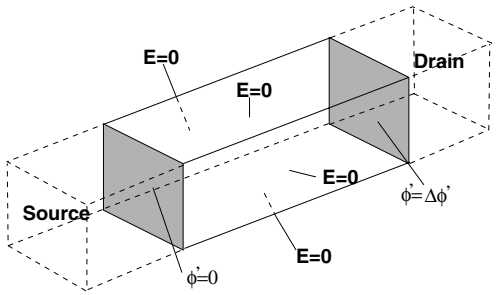

Figure 5. The region considered for the calculation of conductance and associated boundary conditions.

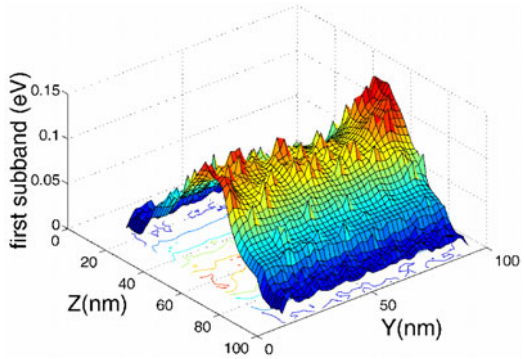

Figure 6. The first-subband profile for a random dopant distribution and $V_{GS} = 0.5$ V.
(This figure is in colour only in the electronic version)

Since, as we have seen, the threshold voltage is also significantly affected by quantum confinement in the channel, we believe that both aspects have to be included in an accurate simulation. Our code allows us to solve the Poisson equation in three dimensions, and therefore to take into account the 'atomistic' distribution of impurities, and to include quantum confinement by solving the Schrödinger equation in the vertical direction. Three-dimensional semiclassical simulations of the effect of random dopants have appeared in the literature [7, 8], and quantum effects have been included with the density-gradient formalism [10], but the two effects have not been considered at the same time.

We have assumed that the implanted ions in the channel show the Poisson distribution. In particular, for each grid-point we have considered the associated volume element and multiplied its volume ΔV by the nominal doping concentration, to obtain the nominal number of dopants in the element $\tilde{N}$. Then, a random number N' has been extracted using a Poisson distribution of average $\tilde{N}$ and divided by ΔV in order to obtain the 'actual' doping concentration in the volume element. The standard deviation of V_T was then obtained by simulating a large number of devices with the same nominal doping, but with different actual dopant distributions. We show in figure 6 the first-subband profile in the channel, where peaks correspond to impurity atoms, and in figure 7 the distribution of threshold voltage computed for an ensemble of 100 nominally identical devices. If V_{Tnom} is the threshold voltage in the case of uniform doping distribution, the mean and the standard deviation of the random variable $V_T - V_{Tnom}$ are respectively equal to 0.6 and 14.5 mV.

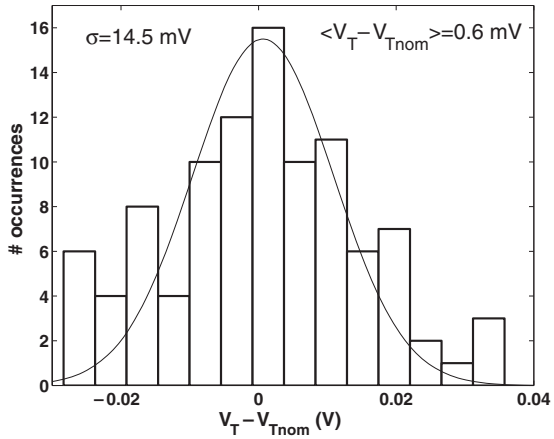

Figure 7. The distribution of threshold voltage obtained from statistical simulations on 100 nominally identical 50 nm MOSFETs.

5. Conclusions

We have developed a three-dimensional Poisson/Schrödinger solver and we have simulated a nanoscale 'well-tempered' MOSFET with channel length of 50 nm. We have shown that for the device considered the solution of the Schrödinger equation can be reduced to the solution of several one-dimensional Schrödinger equations with no practical loss of accuracy and considerable reduction of computational requirements.

Simulations have shown that the threshold voltage shift due to quantum confinement is significant: a quantum simulation is therefore required to obtain results in quantitative agreement with experiments. As geometries are scaled down, the effect of the discrete distribution of dopants also becomes significant and affects important properties such as the threshold voltage. Our code has allowed us to take into account simultaneously the effects of the random distribution of dopants and of quantum confinement in the channel on threshold voltage.

Geometrical dispersion can be another source of threshold voltage fluctuations. As shown in [13], in devices with channel length below 30 nm, oxide fluctuations cause dispersion of V_T comparable to that due to random discrete dopants. This issue requires further investigation.

Acknowledgment

Support from the NANOTCAD Project (IST-1999-10828 NANOTCAD) is gratefully acknowledged.

References

[1] Taur Y and Ning T H 1998 *Fundamentals of Modern VLSI Devices* (Cambridge: Cambridge University Press) p 194
[2] Taur Y *et al* 1997 *Proc. IEEE* **85** 486–504
[3] Fiegna C and Abramo A 1998 *IEEE Trans. Electron Devices* **45** 877–80
[4] Spinelli A, Benvenuti A and Pacelli A 1998 *IEEE Trans. Electron Devices* **45** 1342–9
[5] Abramo A, Cardin A, Selmi L and Sangiorgi E 2000 *IEEE Trans. Electron Devices* **47** 1858–63
[6] Wordelman C J, Aluru N R and Ravaioli U 2000 *CMES* **1** 121–6
[7] Wong H S and Taur Y 1993 *Proc. IEDM 1993* Digest of technical papers pp 705–8
[8] Asenov A 1998 *IEEE Trans. Electron Devices* **45** 2505
[9] Frank D J, Taur Y, Ieong M and Wong H S P 1999 *Symp. on VLSI Circuits* Digest of technical papers
[10] Asenov A, Slavcheva G, Brown A R, Davies J H and Saini S 1999 *IEDM* Technical digest pp 535–8
[11] Inkson J C 1986 *Many Body Theory of Solids—an Introduction* (New York: Plenum)
[12] Trellakis A, Galick A T, Pacelli A and Ravaioli U 1997 *J. Appl. Phys.* **81** 7800–4
[13] Asenov A 2002 *IEEE Trans. Electron Devices* **49** 112